DOI: 10.26599/FSHW.2025.9250563

Contents lists available at SciOpen

Food Science and Human Wellness

journal homepage: https://www.sciopen.com/journal/2097-0765

China Food Publishing Co.

Chitooligosaccharides Ameliorate Glomerular Mesangial Proliferation and Inflammation in IgA Nephropathy by Blocking S1PR1/S1PR3 Pathway

Ran Zhang [a], Xiaoguo Ji [a, d], Yuyan Tang [b], Yijia Chen [a], Zhenwei Yi [a], Jiayang Jin[a, e], Mengyao Zhao [a, d], Hao Yin [c], Haidong He [a, b, *], Liming Zhao [a, c, e, *]

[a] *State Key Laboratory of Bioreactor Engineering, East China University of Science and Technology, Shanghai 200237, China*

[b] *Department of Nephrology, Minhang Hospital, Fudan University, Shanghai 201199, China*

[c] *Organ Transplant Center, Chang Zheng Hospital, Shanghai 200003, China*

[d] *Shanghai Frontiers Science Center of Optogenetic Techniques for Cell Metabolism, School of Pharmacy, East China University of Science and Technology, 130 Mei Long Road, Shanghai 200237, China*

[e] *Shanghai Collaborative Innovation Center for Biomanufacturing Technology (SCICBT), Shanghai 200237, China*

ABSTRACT: IgA nephropathy (IgAN) is a common primary glomerulonephritis characterized by metabolic abnormalities that accelerate disease progression. Chitooligosaccharides (COS) exhibit notable regulatory effects on metabolism and inflammation, yet their therapeutic effects and underlying mechanisms in IgAN remain unexplored. This study identified distinct serum metabolic profiles in IgAN patients, distinguishing them from healthy controls. Notably, a significant increase in the metabolite sphingosine-1-phosphate (S1P) not only indicated the severity of IgAN progression but also induced IgAN-like pathological phenotypes in glomerular mesangial cells (including excessive proliferation and inflammation). COS with specific degree of polymerization significantly inhibited the G2/M phase of the cell cycle in glomerular mesangial cells while promoting S-phase arrest and apoptosis ($P < 0.05$), collectively suppressing the excessive cellular proliferation induced by S1P. Additionally, COS reduced the levels of inflammatory factors including IL-6, IL-1β, TNF-α, and MCP-1 ($P < 0.05$) in both cell and animal models. Mechanistically, COS alleviated S1P-induced cellular effects and improved renal function and inflammation by suppressing the expression and activity of S1PR1 and S1PR3, which was similar with the effects of S1P antagonist FTY720. Overall, this study highlighted COS as a potential functional food for mitigating IgAN progression by targeting S1P signaling.

Keywords: Chitooligosaccharides; IgA nephropathy; Sphingosine-1-phosphate; Sphingosine-1-phosphate receptor

1. Introduction

IgA nephropathy (IgAN) is a prevalent cause of glomerulonephritis worldwide [1,2], with approximately 20-40% of IgAN patients progressing to end-stage renal disease (ESRD) within 20 years without targeted therapy [3,4]. The pathology of IgAN is primarily characterized by the deposition of pathogenic immune complexes (ICs) containing IgA within the glomerulus. This process is triggered by the recognition of galactose-deficient IgA1 (Gd-IgA1) by autoantibodies, which ultimately leading to renal injury [5,6]. The

***Corresponding author**
zhaoliming@ecust.edu.cn (LM. Z.); chinahhd@sina.com (HD. H.)

Received 21 November 2024
Received in revised from 2 January 2025
Accepted 24 January 2025

primary pathological features of IgAN include immune complex deposition, mesangial cell proliferation, and glomerular inflammation. However, due to an incomplete understanding of IgAN's pathogenesis, the targets for IgAN prevention and intervention are not yet clear. Therefore, it is imperative to elucidate the pathogenesis of IgAN further and develop reliable therapeutic interventions based on its pathological characteristics.

Within the realm of kidney disease, there is increasing focus on understanding the significant influence of metabolic factors. Current research focuses on screening and identifying potential biomarkers that reflect metabolic irregularities, providing targets for disease diagnosis or novel drug development [7-9]. Previous studies employing metabolomics have identified metabolic disturbances associated with IgAN [10-12]. Abnormalities in serum terpenoid quinone biosynthesis (e.g., ubiquinone), and glycerophospholipid metabolism were observed in IgAN patients compared to healthy controls [13]. Additionally, IgAN patients exhibited disturbances in unsaturated fatty acids (linoleic acid and arachidonic acid) metabolism and tryptophan metabolism, leading to an active immune-inflammatory response [10]. Abnormal glycine levels in the urinary metabolites of IgAN patients were correlated with IgAN progression. Notably, high glycine levels can ameliorate tumor necrosis factor alpha-induced inflammatory signaling, suggesting its potential as a protective biomarker for IgAN [14]. Research has also identified correlations between the gut microbiota community structure and metabolic irregularities, including lipid, carbohydrate, and nucleotide metabolism, in IgAN animal models. These findings suggested a potential role for gut microbiota in diagnosing and predicting IgAN progression [15-18]. These findings collectively highlighted the intimate link between metabolic dysfunction and the development of IgAN. However, validated metabolic targets specific to IgAN are currently lacking, necessitating further investigations in clinical or animal models for deeper insights. Moreover, targeted interventions based on these discoveries have yet to be developed.

Chitooligosaccharides (COS) are oligomers with a degree of polymerization ranging from 2 to 10, derived from natural chitosan. COS exhibited excellent activities in regulating immunity, inflammation, glycolipid metabolism, and adjusting intestinal microecology [19-21]. Moreover, COS displayed a clear structure-activity relationship, with specific degrees of polymerization (DPs) shown to mitigate renal damage and pathological markers in diabetic nephropathy. COS alleviated oxidative stress by increasing renal superoxide dismutase, glutathione peroxidase, and catalase activities by 45%, 37%, and 50%, respectively ($P < 0.05$), while decreasing malondialdehyde content by 30% ($P < 0.05$) [22]. COS with varying DPs had also shown efficacy in alleviating DSS-induced colitis. COS6 reduced colonic MPO levels to normal ((144.1 ± 10.23) pg/mL, $P < 0.05$) and restored the levels of protective tryptophan metabolites, such as indole-3-acetic acid and indole-3-carbaldehyde, in the cecum ($P < 0.05$) [23]. Given their demonstrated effects on inflammation and metabolic balance, COS may hold considerable potential for mitigating the progression of IgAN.

This study aimed to investigate the effects and mechanisms of COS on IgAN and to explore potential metabolic regulatory strategies to improve disease prognosis. The effective metabolic biomarker in IgAN patients was identified and the roles in proliferation and pro-inflammatory responses were investigated in

glomerular mesangial cells and IgAN animal models. COS with a specific DP was selected which can effectively mitigate IgAN-related pathology, followed by efficacy validation in animal models. The results demonstrated that COS with specific DP exerted effects similar to those of sphingosine-1-phosphate (S1P) antagonist FTY720. These effects effectively modulated the pathological phenotypes resulting from S1P metabolic disturbances and improved renal function by inhibiting the S1PR1/S1PR3 pathway. In conclusion, this study supported the potential of COS as a functional food for mitigating the progression of IgAN.

2. Materials and methods

2.1 Ethics statement

The experiment involving human subjects was conducted in accordance with the Declaration of Helsinki (as revised in 2013). All procedures were carried out following protocols approved by the Ethics Committee of the East China University of Science and Technology (ECUST) (Ethical No. ECUST-2022-110), and the Ethics Committee of the Minhang Hospital, Fudan University (Ethical No. 2021-056-01K). All participants provided informed consent.

All the animal experiments were performed in accordance with the Guidelines for the Care and Use of Laboratory Animals published by the United States National Institute of Health (NIH, Publication No. 85-23, 1996). All the animal experiments were approved by the Ethics Committee of the East China University of Science and Technology and followed the Guide for the Care and Use of Laboratory Animals (Ethical No. ECUST-2023-051).

2.2 Subject recruitment and clinical sample collection

A total of 55 individuals (aged 20-60) were recruited, including 35 patients with IgAN and 20 healthy controls (HCs), who were grouped by sex and age. All patients with IgAN were diagnosed via kidney biopsy, and HCs were recruited at the physical examination center of Minhang Hospital, affiliated with Fudan University in Shanghai, China. The participants signed an informed consent form. The cohort consisted of 35 patients with IgAN and 20 HCs. The exclusion criteria for the IgAN group were as follows [24,25]: (i) fewer than 10 glomeruli; (ii) diagnosis of other diseases (e.g., secondary IgAN, autoimmune disorders, hyperlipidemia, non-alcoholic fatty liver, acute myocardial infarction, diabetes mellitus, and digestive tract disease); and (iii) reported use of immunosuppressive agents, glucocorticoids, and antibiotics within six months. Exclusion criteria for the HC group were diabetes, hypertension, obesity, inflammatory bowel disease, and abnormal liver or renal function. The validation cohort included in further studies consisted of 27 IgAN patients and 15 HCs. Clinical information was collected from all IgAN patients and corresponding information was collected from healthy volunteers.

Blood samples from patients were collected during early hospitalization, while samples from HCs were collected during physical examination. The serum samples were obtained by centrifugation of blood samples with the condition of 3000 × *g* at 4 ℃ for 15 min, the supernatant was used for further studies. Fresh fecal and urine samples were collected simultaneously in sterile containers for further analysis.

2.3 Metabolites extraction and untargeted metabolomics analysis

The sample pre-treatment methods were modified from the previously reported method [26,27]. The specific procedures were as follows. To effectively remove protein macromolecules and improve metabolite coverage, a pre-cooled 50% (v/v) methanol/acetonitrile mixture (300 μL) was added to each sample (100 μL). The prepared 2-chloro-L-phenylalanine in methanol (10 μL, 0.3 mg/mL) was used as the internal standard. The mixture was vortexed for 30 seconds and placed at -20 ℃ for 30 min to cool down, which was then centrifuged at 13000 × *g* for 15 min (4 ℃). The supernatant obtained was dried with a vacuum dryer at a low temperature and then re-dissolved in a pre-cooled 80% (v/v) methanol/water mixture (300 μL). The supernatant was finally collected and filtered through a 0.22 μm filter for further analysis. Fecal samples from each subject were weighed (30 mg), and 600 μL of the pre-cooled 80% (v/v) methanol/water mixture was added, with 2-chloro-L-phenylalanine (Sigma-Aldrich, USA) in methanol (20 μL, 0.3 mg/mL) added as the internal standard. Then the mixture was cooled and ground for 2 min at 60 Hz for full metabolite extraction. After centrifugation at 13000 × *g* for 15 min (4 ℃), 300 μL of the supernatant was removed and dried in a vacuum dryer at a low temperature. Then, 300 μL of the pre-cooled 50% (v/v) methanol/water mixture was added to reconstitute the dried samples, the process for the supernatant was the same as that of the serum samples. The quality control (QC) sample for each system was prepared by mixing the same volume of each sample for assessment, and methanol was used as the blank sample.

Shimadzu Nexera UHPLC LC-30A system (Shimadzu, Japan) was used for metabolome separation, and Q-Exactive quadrupole-Orbitrap mass spectrometer was used for further structural identification of the metabolites. The detection method was performed with reference to the literature with slight modifications [23,27,28]. Specifically, mobile phases A (water with 0.1% formic acid, v/v) and B (acetonitrile with 0.1% formic acid, v/v) were prepared, and the instrument was then vented for 5 min. The prepared samples were arranged in groups, and QC and blank samples were randomly inserted into the sequence samples for quality control. The column temperature was set at 40 ℃, the injection volume was 2 μL, and the flow rate was set at 0.35 mL/min. The chromatographic gradient optimized for this study was 0-2 min, 95% A; 2-10 min, 5% B → 80% B; 10-14 min, 80% B → 100% B, 15-16 min, 100% B → 5% B. The mass spectrometry conditions were set as follows: sheath gas flow rate was 40 arbs, auxiliary gas flow rate was 10 arbs, full MS resolution was 70,000, MS/MS resolution was 17,500, capillary temperature was 320 ℃, probe heater temperature was 350 ℃, spray voltage was 3.5 kV in positive and -3.5 kV in negative mode. All samples were tested in the positive and negative ion modes. The qualitative analysis and peak area normalization of raw data were then processed to obtain the data matrix, which was further analyzed using the SIMCA® 14.1 software (Umetrics AB, Umea, Sweden).

2.4 Screening of the serum biomarker and linear correlation analysis

To integrate multiple holographic datasets (including metabolomes of serum, feces, urine, clinical indicators, and inflammatory indicators) obtained from the same individual, a multivariate dimensionality reduction method was initially applied. Linear combinations of variables within each omics dataset were used

to determine the latent components. To further identify the metabolic biomarkers of IgAN, the screened differential metabolites were analyzed for association with clinical indicators and inflammatory factors using Mantle's test and Spearman's rank correlation analysis. Linear correlation analysis was also performed between the peak values of serum S1P and eGFR, Scr, and 24h-Upro to determine the indicative role of serum S1P in IgAN.

2.5 Cell culture and treatments

Mouse glomerular mesangial cells (SV40 MES 13) were purchased from Procell Life Science & Technology Co., Ltd. S1P and FTY720 were purchased from MCE (HY-108496; HY-12005; Monmouth Junction, NJ, USA) and dissolved in DMSO for further use. COS with a single DP COS4 was prepared in our laboratory [27] (Supplementary Fig. S4). SV40 MES 13 cells were cultured in DMEM/F-12 (3:1) (Gibco, USA) supplemented with 10% fetal bovine serum (Gibco, USA), and incubated at 37 ℃ with 5% CO_2. SV40 MES 13 cells were treated with different concentrations of S1P after 24h of serum-free starvation to induce a proliferative and inflammatory state. Cells were selected to be treated with COS of DP4 (1 μmol/L, 5μmol/L, 10 μmol/L) or FTY720 (5 μmol/L) simultaneously with S1P after serum-free starvation.

2.6 MTT assay

The effects of different concentrations of S1P on the viability of SV40 MES 13 cells were measured using the MTT assay. The 96-well plates were homogeneously inoculated with 1×10^4 cells/well and subjected to 24-hour serum-free starvation. Then the cells were treated with different concentrations of S1P and cultured for 24h, 48h, and 72h, respectively. 10 μL of MTT (at a final concentration of 0.5 mg/mL) was added to each well and incubated at 37 ℃ for 4h. The supernatant was then carefully removed from each well, and 100 μL of DMSO was added to dissolve all the formazan. Absorbance was measured using a microplate reader (Synergy HT, Biotek, USA) at 490 nm. After determining the optimal S1P treatment conditions, the effects of co-treatment of COS or FTY720 with S1P on cell viability were determined using the MTT assay described above.

2.7 EdU staining

SV40 MES 13 cell proliferation treated by S1P, FTY720, and COS was detected using BeyoClick™ EdU cell proliferation kit with Alexa Fluor 488 (Beyotime Biotechnology, Shanghai, China). 5×10^5 cells/well were homogeneously inoculated in six-well plates and subjected to serum-free starvation for 24h. EdU working solution (final concentration 10 μmol/L) was added to each well, then incubated for 2h, fixed with 4% paraformaldehyde for 15 min, and incubated with immunostaining permeabilization solution for 10 min. Then, the Click reaction solution was added to each well for 30 minutes at room temperature (20-25 ℃) and protected from light. The cells were incubated with Hoechst 33342 at room temperature (20-25 ℃) and protected from light for 10 min, followed by observation under a fluorescence microscope.

2.8 Flow cytometry analysis

Cell cycle and apoptosis analysis kit and Annexin V-FITC apoptosis detection kit (Beyotime Biotechnology, Shanghai, China) were used for flow cytometry analysis in different treated cells. SV40 MES 13 cells were digested with trypsin, resuspended in pre-cooled 70% ethanol, and fixed overnight at 4 ℃. The fixed cells were resuspended in propidium iodide staining solution (containing RNase A), warmed in a light-protected bath at 37 ℃ for 30 minutes, and then used for the assay. Cells for apoptosis assay were gently resuspended with Annexin V-FITC conjugate and stained with Annexin V-FITC and propidium iodide staining solution, respectively. Cells were incubated at room temperature (20-25 ℃) for 10 minutes in the absence of light before being used for flow cytometry.

2.9 Animal experiment

Thirty 5-week male Balb/c mice (20 ± 2) g were housed in a specific pathogen-free (SPF grade) clean animal house with a 12h light/dark cycle, with room temperature at (21 ± 2) ℃. All mice were randomized after one week of acclimatization and were divided into five experimental groups (n = 6): (a) Control group (PBS), (b) IgAN group, (c) FTY720 group (1mg/kg/day FTY720), (d) COS group (150 mg/kg/day COS), (e) FTY720+COS group (1mg/kg/day FTY720+150 mg/kg/day COS). All interventions were performed at the end of the modeling. The IgAN mice model was constructed using the bovine serum albumin (BSA) + lipopolysaccharides (LPS) + carbon tetrachloride (CCl_4) method [29-31]. Specifically, except for the control group, mice were gavaged with BSA (800 mg/kg) every other day for 8 weeks, and subcutaneously injected with castor oil (0.5 mL) and CCl_4 (0.1 mL) once a week for 9 weeks, and were injected with 0.05 mg LPS by tail vein in the 6th and 8th weeks, respectively. The control group was treated with the corresponding dose of PBS at the appropriate time. FTY720 (1mg/kg/day) [32-34] and COS (150 mg/kg/day) [21,35] were administered by daily gavage for six weeks. At the end of the experiment, 24-hour urine samples from all groups were collected using the metabolic cages. Blood samples and other biological samples, including kidneys, intestinal tissues, and feces, were carefully collected for further analysis.

2.10 Histology and immunofluorescence analysis

Periodic acid-Schiff (PAS) staining was used for pathological analysis of kidneys. Briefly, kidney tissues fixed in 4% paraformaldehyde were paraffin-embedded, sectioned, and stained with PAS. The final image acquisition was performed using an upright optical microscope (Nikon Eclipse E100, Japan). Immunofluorescence analysis was also performed to identify the IgA deposition and the proliferative factors secretion, including vascular endothelial growth factor (VEGF) and platelet-derived growth factor (PDGF) in the kidneys of different treatment groups. Kidney tissue sections were deparaffinized and rehydrated and then antigenically repaired. The fixed sections were sealed with 3% BSA solution for 30 min and incubated with primary antibodies anti-mouse IgA (bs-0774R, Bioss, Beijing, China, 10 μg/mL), rabbit anti-mouse PDGF (GB11261, Servicebio, 5 μg/mL), and rabbit anti-mouse VEGF (GB14165, Servicebio, 5 μg/mL) at 4 ℃ overnight, followed by incubation with fluorescence-labeled secondary antibody Alexa Fluor® 488-conjugated Goat Anti-Rabbit IgG (H+L) (GB25303, Servicebio, 5 μg/mL) at room temperature without

light for 50 min. The nucleus was subsequently restained with DAPI and mounted for imaging. Images were acquired and analyzed using a fluorescence microscope (Nikon Eclipse C1, Japan).

2.11 ELISA assays

ELISA kits (MLBIO Biotechnology Co. Ltd, Shanghai, China) were used to detect the indices in serum and kidney tissues. Blood samples from human subjects and mice were centrifuged at 3000 × *g* for 15 min at 4 ℃, and serum was collected for further testing. Cytokine levels, including IgA1, interleukin-4 (IL-4), IL-6, IL-17, tumor necrosis factor-α (TNF-α), transforming growth factor-β (TGF-β), and S1P levels were measured in human serum samples. S1P levels were detected in serum samples obtained from mice. The cellular inflammatory factors (IL-6, TNF-α, IL-1β, and MCP-1) in the cell culture supernatant and the proliferation factors (VEGF and PDGF) in the cell culture supernatant and cells were determined. In addition, the levels of IL-6, TNF-α, IL-1β, and MCP-1, Sphingosine kinase 1 (SPHK1), S1PR1, and S1PR3 in mice kidney tissues were detected. Accurately weighed kidney tissues were homogenized, ground using a grinder at 4 ℃, and centrifuged at 1000 × *g* for 15 min. The supernatants were collected for index assays and quantification of protein concentration using the enhanced BCA protein assay kit (Beyotime Biotechnology, Shanghai, China). All assays were performed according to the manufacturer's instructions.

2.12 Quantitative real-time PCR (qPCR) analysis

Total RNA from cells and tissues was extracted according to the manufacturer's instructions for the FastPure Cell/Tissue Total RNA Isolation Kit V2 (Vazyme, Nanjing, China), and then was reverse transcribed according to the manufacturer's instructions for the HiScript II Q RT SuperMix for qPCR (+gDNA wiper) (Vazyme, Nanjing, China). The qPCR analysis was performed using SYBR according to AceQ® qPCR SYBR Green Master Mix (Vazyme, Nanjing, China). The mRNA expression levels of each gene were obtained by normalization to GAPDH and calculated using the ΔΔCT method. Primers for the genes used are listed in Supplementary Table S4.

2.13 Molecular docking

To investigate the mode of interaction between COS and S1P receptors (S1PR1/S1PR3), the molecular structure of COS was downloaded from PubChem (PubChem CID:70702330). The S1PR1 protein (PDB code: 7VIE) and S1PR3 (PDB code: 7C4S) were downloaded from the Protein Data Bank (RCSB PDB Homepage). The natural ligand (S1P) was removed from the crystal structures of S1PR1 and S1PR3 proteins. Docking centers of proteins based on the natural ligand were identified using AutoDock Tools 1.5.6, and docking results were further analyzed and visualized using PyMOL [21]. The molecular interactions visualization and molecular dynamics simulations were performed using the Desmond (Schrödinger Release 2018-4) [36].

2.14 Statistical analyses

All data was presented as mean ± standard deviation. Student's *t*-test was used to compare the differences between two groups, and one-way ANOVA was used to compare the differences between

multiple groups. Spearman's correlation analysis and Mantle's test were used for correlation analysis. Statistical analyses were performed using GraphPad Prism 7.0 (GraphPad Software, San Diego, CA, USA). Data was considered statistically significant at $P < 0.05$.

3. Results

3.1 Clinical characteristics of the recruited participants

All participants hailed from East China. Baseline and clinical data were summarized for 55 enrolled volunteers and 42 volunteers who were eventually included in the study (Fig. 1A, Supplementary Fig. S1). There were no significant differences between the IgAN and HC groups regarding baseline parameters, including age and body mass index (BMI) ($P > 0.05$) (Fig. 1A (1)-(2)). We performed a contingency analysis (Chi-square test) on the gender distribution, and the results also showed no significant difference (55 volunteers, $p = 0.508$; 42 volunteers, $p = 0.747$). Similarly, clinical indicators like total cholesterol (TC), triglyceride (TG), and C-reactive protein (CRP) levels displayed no significant disparities between the IgAN and HC groups ($P > 0.05$) (Fig. 1A (10)-(12)). Thus, the influence of dyslipidemia on this study can be ruled out. Notably, several key indicators exhibited substantial differences in the IgAN group. Specifically, serum creatinine (Scr) ($P < 0.001$), cystatin C (Cys-C) ($P < 0.001$), blood urea nitrogen (BUN) ($P < 0.05$), hemoglobin A1c (HbA1c) ($P < 0.001$), and 24-hour urine protein (24h-Upro) ($P < 0.05$) levels were significantly elevated. In contrast, the estimated glomerular filtration rate (eGFR) ($P < 0.001$) was notably reduced (Fig. 1A (3)-(8)).

The prevailing understanding attributes renal injury in IgAN to the abnormal production and buildup of Gd-IgA1, leading to B-cell stimulation due to intestinal mucosal damage and consequent inflammation [37,38]. To assess IgA1 levels and inflammatory status in IgAN patients, the levels of serum IgA1 and inflammation cytokines (IL-4, IL-6, IL-17, TNF-α and TGF-β) between the two groups were analyzed (Fig. 1B). The findings indicated significantly elevated serum levels of IgA1 ($P < 0.001$), IL-4 ($P < 0.01$), TNF-α ($P < 0.001$), IL-6 ($P < 0.001$), and IL-17 ($P < 0.01$) in IgAN patients. However, TGF-β levels did not exhibit notable differences between the two groups ($P > 0.05$), suggesting the presence of systemic inflammation in IgAN patients.

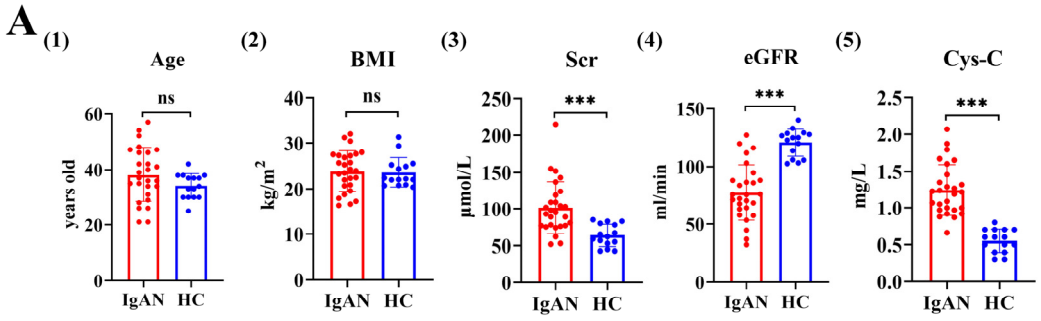

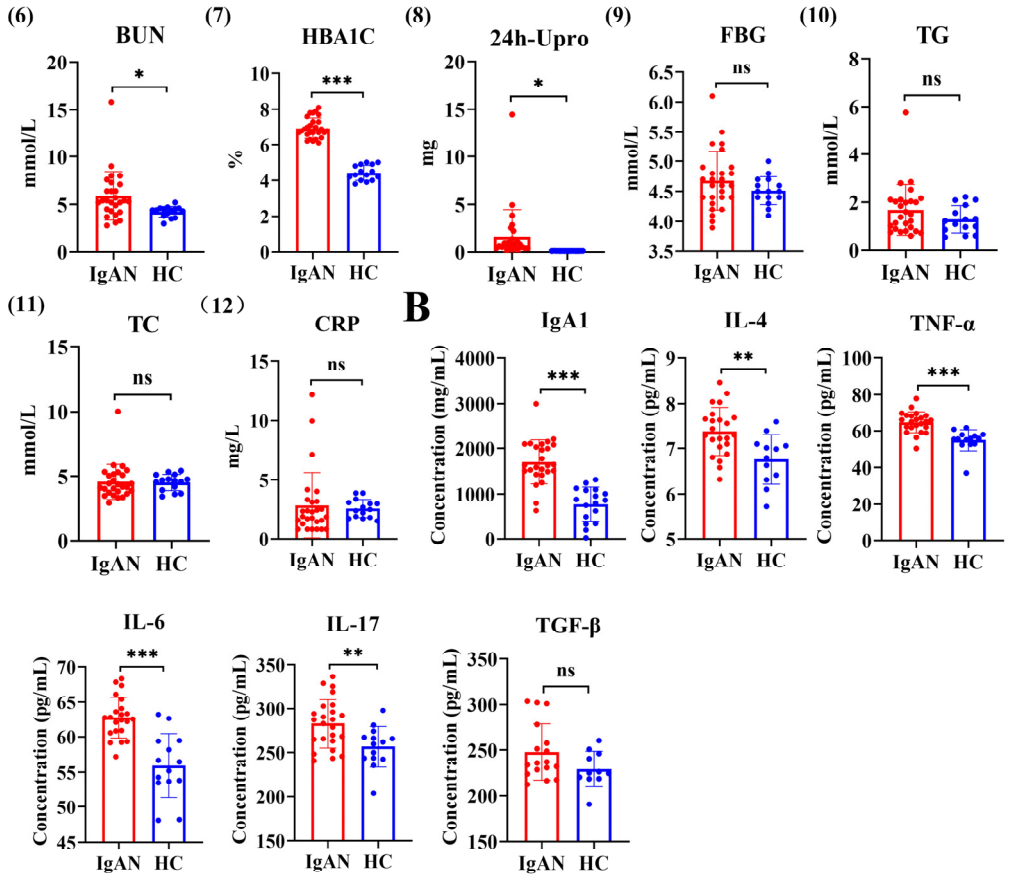

Fig. 1. Baseline and clinical indices of the 42 volunteers included in the study. (A) (1-12) The basic and clinical indicators of 42 volunteers who were finally enrolled in the study according to the inclusion and exclusion criteria. (B) The expression of immunity and inflammatory factors in the serum of the two groups. *$P < 0.05$, **$P < 0.01$, ***$P < 0.001$, and ns represented $P > 0.05$.

3.2 Serum metabolomic profiles could clearly distinguish IgAN patients from healthy controls

To delineate the metabolic phenotype of individuals with IgAN and identify pertinent biomarkers, the study performed comprehensive untargeted metabolomic analyses on all subjects' biological samples, including serum, feces, and urine. Principal component analysis (PCA) (Fig. 2A-C) and partial least squares discrimination analysis (OPLS-DA) (Fig. 2D-F) were employed to cluster all metabolomic data. Distinct differences emerged between the metabolomes of the IgAN and HC groups across serum, fecal, and urine systems, with more pronounced metabolic variations evident in serum samples. Supervised clustering in serum samples revealed significant distinctions in the metabolic profiles of IgAN patients compared to the HC group (Fig. 2A, D). This suggested that alterations in the serum metabolome might serve as a crucial indicator for IgAN. Furthermore, these disparities indicated potential damage to the intestinal mucosa in IgAN patients, facilitating the entry of specific microbial metabolites into the bloodstream and influencing disease progression.

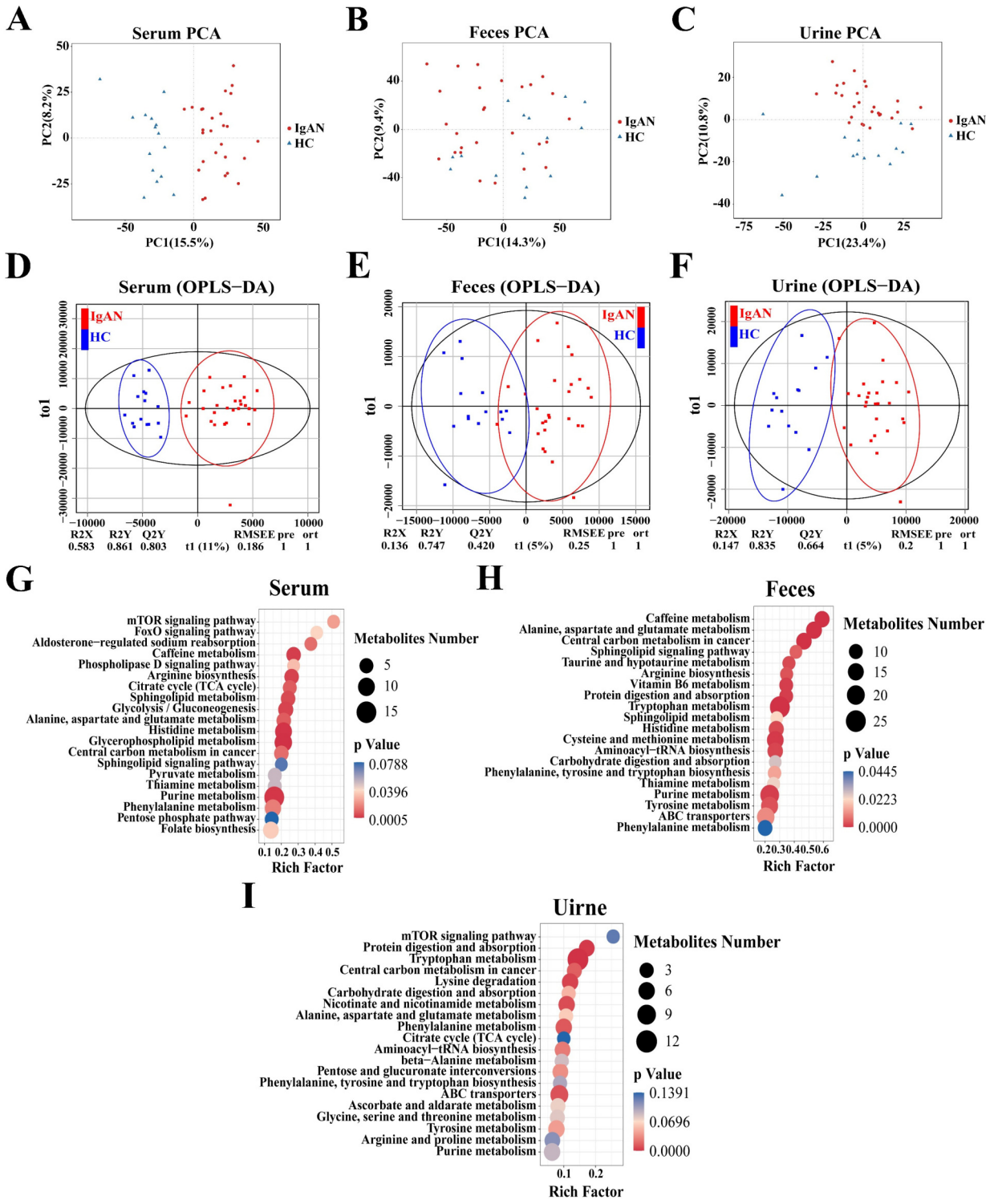

Fig. 2. Clustering analysis of serum, fecal, and urine metabolites and the functional pathways enriched between the IgAN and HC groups. (A-C) From left to right were the PCA analyses of the serum, feces, and urine metabolomes, respectively. (D-F) From left to right were the OPLS-DA analyses of the serum, feces, and urine metabolomes, respectively. (G-I) From left to right are the KEGG pathway enrichment analyses of the serum, fecal, and urine differential metabolites, respectively. The X-axis represented the enrichment factor, and the Y-axis represented the pathways. The red represented the IgAN group, and blue represented the HC group.

The KEGG functional pathway enrichment analysis was conducted on the complete metabolomic profiles in the IgAN and HC groups (Fig. 2G-I). The results showed that the pathways significantly enriched in serum were closely related to lipid and energy metabolism pathways, and signal transduction pathways (Fig. 2G), such as sphingolipid metabolism ($P < 0.01$), glycerophospholipid metabolism ($P < 0.001$), and

glycolysis/glycogenesis ($P < 0.001$). Differential metabolites in feces were involved in functional pathways related to protein and amino acid (especially aromatic amino acids) metabolism (Fig. 2H), including protein digestion and absorption ($P < 0.01$), and tryptophan metabolism ($P < 0.001$). Fecal differential metabolites were also involved in metabolic pathways associated with lipid signaling, including sphingolipid metabolism ($P < 0.05$) and sphingolipid signaling pathways ($P < 0.01$). In contrast, the metabolic pathways enriched for urine differential metabolites were mainly associated with protein and amino acid metabolism, with aromatic amino acid metabolism being of significance (Fig. 2I). In addition, the central carbon metabolism pathway was significantly enriched in all three systems, which may indicate disturbed energy metabolism in IgAN patients. Overall, the metabolic pathways enriched in serum, fecal, and urine metabolites were mainly related to energy metabolism, lipid signaling-related pathways, and amino acid (especially aromatic amino acid) metabolism.

3.3 S1P as a differential biomarker of IgAN which was closely correlated with renal functions

The differential metabolites in the serum, feces, and urine systems of the IgAN group were screened and identified using OPLS-DA analysis ($P < 0.05$, and VIP > 1). These metabolites were further validated through secondary spectra and manual screening. A total of 41 differential metabolites in serum, 24 differential metabolites in feces, and 24 differential metabolites in urine were identified (Fig. 3A, Supplementary Fig. S2A-S3A, Supplementary Table S1-S3). To evaluate the predictive capability of these distinct metabolites for IgAN, receiver operating characteristic (ROC) analysis was employed to identify and analyze the aforementioned metabolites. An area under the curve (AUC) value exceeding 0.7 generally indicates superior diagnostic performance [39,40]. Consequently, several metabolites with diagnostic potential were further scrutinized across serum, fecal, and urine systems (Fig. 3B, Supplementary Fig. S2B-S3B). Notably, serum-based differential metabolites exhibited greater significance and relevance as diagnostic indicators for IgAN. Specifically, S1P (AUC=0.995) displayed the most substantial diagnostic value.

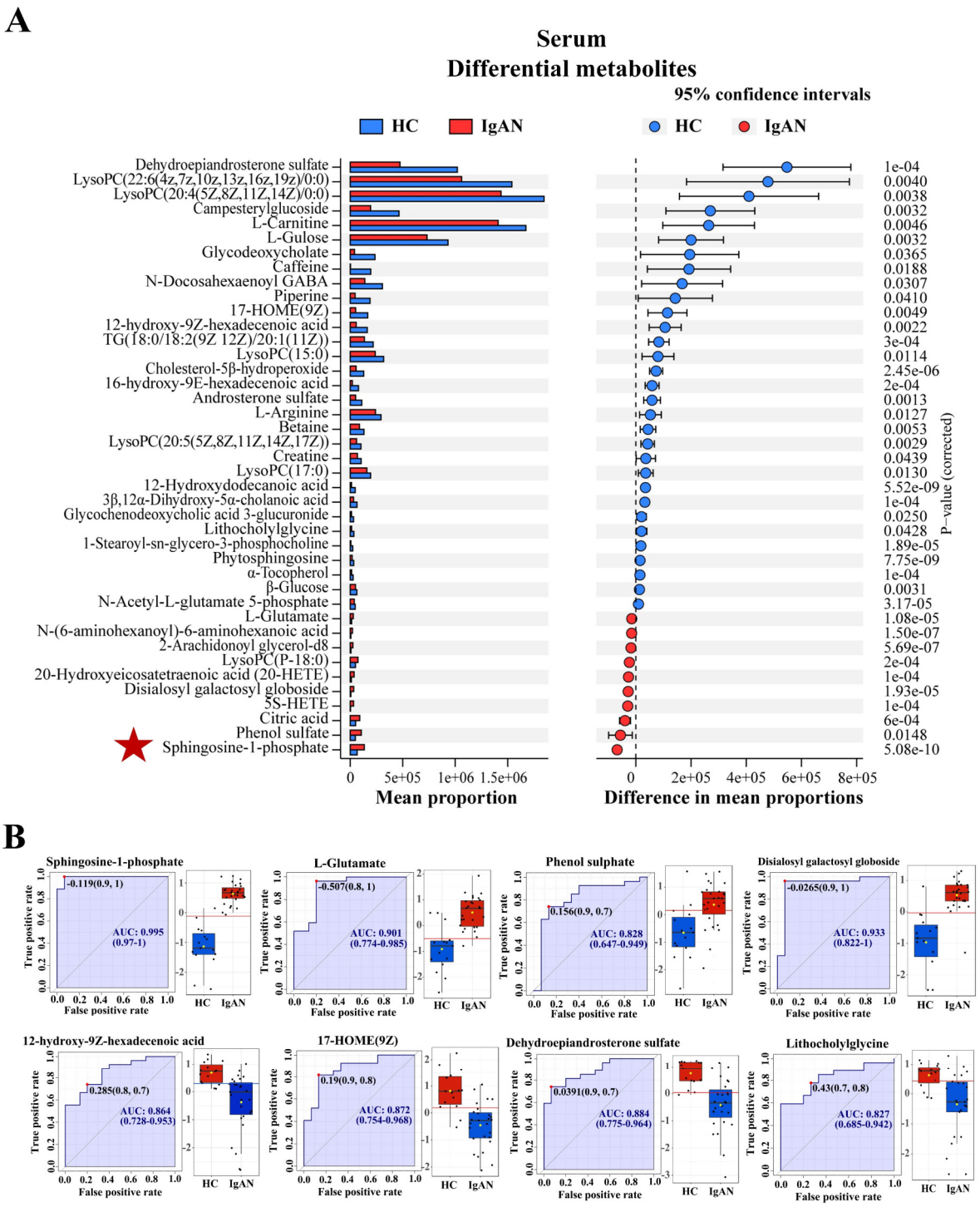

Fig. 3. Differential metabolite screening and ROC analysis of the serum metabolome between the IgAN and HC groups. (A) The statistical analysis of differential metabolites between the two groups at 95% confidence intervals in serum. (D) The ROC curves for the differential metabolites with AUC values greater than 0.7 in the serum.

The correlation analysis of differential metabolites and clinical indicators of IgAN was performed (Fig. 4A-B). Overall, serum metabolites had a closer correlation with IgAN clinical indicators, particularly eGFR, Cys-C, HbA1c, and IgA1. It was hypothesized that abnormalities in serum metabolic function would directly influence the course and severity of IgAN. Some of the metabolites that were significantly elevated in IgAN showed certain correlation with inflammatory indicators (Fig. 4B). Among them, S1P showed significant correlations with 24h-Upro (r = 0.740, P < 0.001), Cys-C (r = 0.694, P < 0.001), HbA1c (r = 0.747, P < 0.001), IgA1 (r = 0.755, P < 0.001), BUN (r = 0.483, P < 0.01), Scr (r = 0.392, P < 0.05), IL-4 (r = 0.433, P

< 0.01), TNF-α (r = 0.422, P < 0.01), IL-17 (r = 0.361 P < 0.05), IL-6 (r = 0.509 P < 0.01), and eGFR (r = -0.557, P < 0.001), which were highly indicative. In addition, the linear correlation analysis showed significant positive correlations between S1P and Scr (p = 0.0265) and 24h-Upro (p = 0.0013) and a significant negative correlation with eGFR (p = 0.0011) (Fig. 4C-E). The quantitative detection of serum S1P in the IgAN and HC groups also showed significantly higher levels of S1P in the IgAN group (P < 0.001) (Fig. 4F).

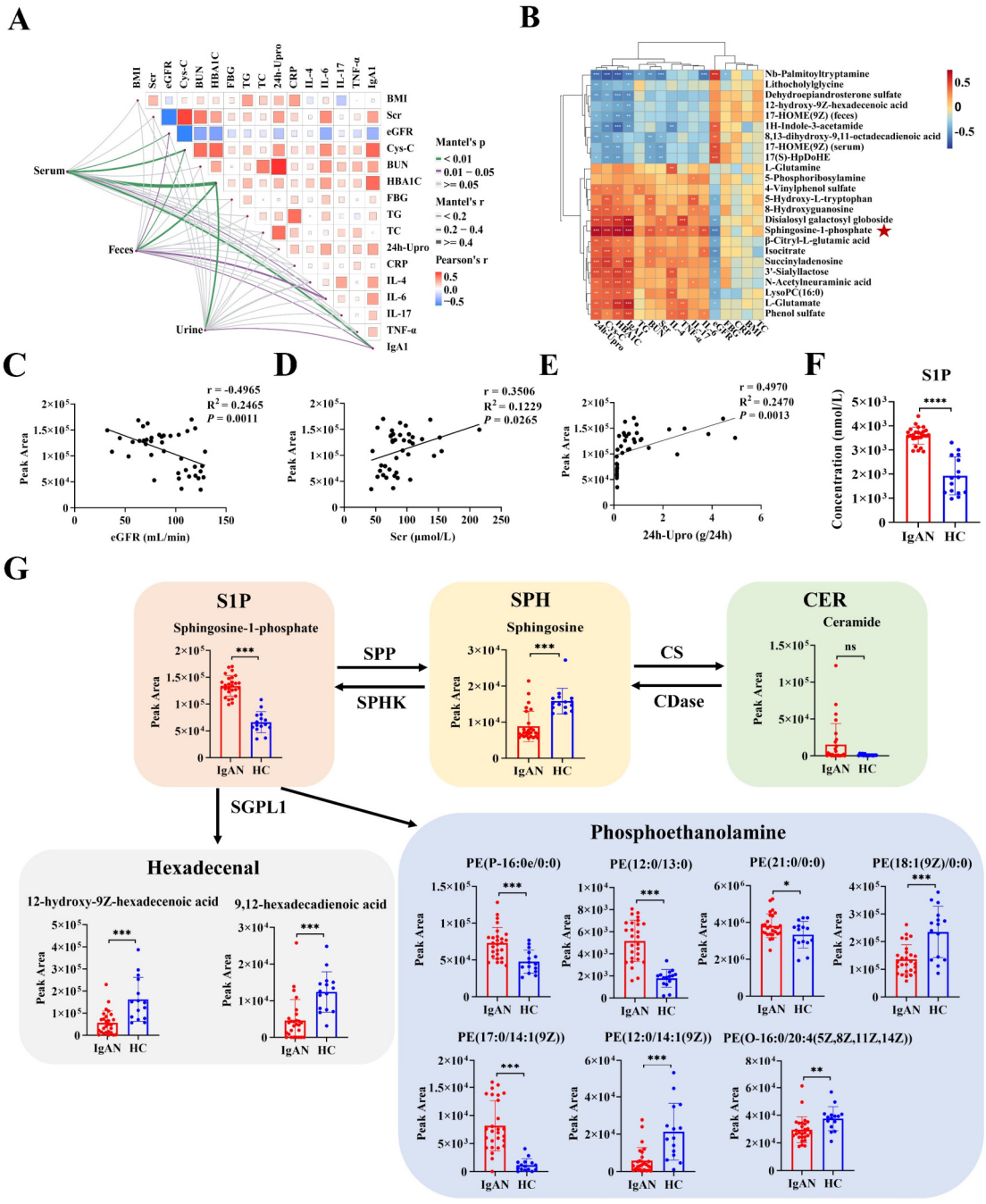

Fig. 4. Identification of the important indicative role of metabolite S1P on IgAN. (A) Mantel test analysis of the differential metabolite profiles of the IgAN and HC groups with clinical indicators and levels of immunoinflammatory factors. (B) Heatmap analysis of the correlation between the metabolites screened in serum, fecal, and urine systems and clinical and immuno-inflammatory indicators. (C-E) Linear correlation analyses of S1P with eGFR, Scr, and 24h-Upro. (F) Quantification of S1P levels in serum of IgAN (n=27) and HC groups (n=15). (G) The metabolic pathway of S1P and comparison of serum metabolites associated with S1P metabolism between IgAN and HC groups. *P < 0.05, **P < 0.01, ***P < 0.001, and ns represented P > 0.05. Abbreviations: CER, ceramide; SPH, sphingosine; CS, ceramide synthase; CDase, ceramidase; SPP, sphingosine phosphatase; SPHK, sphingosine kinase; SGPL1, sphingosine-1-phosphate lyase 1.

Based on the metabolic pathway of S1P (Fig. 4G), we further analyzed other metabolites associated with sphingolipid metabolism in serum, fecal, and urine metabolomic data. No differences were observed in fecal and urinary metabolites. In contrast, in serum metabolites, a significant decrease in sphingosine (SPH) levels ($P < 0.001$) was found in the IgAN group, with no substantial change in ceramide levels ($P > 0.05$). And the levels of hexadecenoic acid, including 9,12-hexadecadienoic acid ($P < 0.001$) and 12-hydroxy-9Z-hexadecenoic acid ($P < 0.001$), were significantly reduced in the IgAN group. Regarding phosphoethanolamine, considerably higher levels of PE (P-16:0e/0:0) ($P < 0.001$), PE (21:0/0:0) ($P < 0.05$), PE (12:0/13:0) ($P < 0.001$), and PE (17:0/14:1(9Z)) ($P < 0.001$) were found in the IgAN group, whereas PE (18:1(9Z)/0:0) ($P < 0.001$), PE (O-16:0/20:4(5Z,8Z,11Z,14Z)) ($P < 0.01$) and PE(12:0/14:1(9Z)) ($P < 0.001$) levels were significantly reduced. Therefore, the pronounced dysregulation of S1P-related metabolism in IgAN might be closely associated with the disease's pathogenesis.

3.4 COS inhibited S1P-induced glomerular mesangial cell proliferation

To investigate the role of the metabolic target S1P in the pathological processes of IgAN, we conducted *in vitro* experiments. SV40 MES 13 cells were exposed to varying concentrations of S1P for 24h, 48h, and 72h to evaluate cell viability and proliferation. Notably, 1 μmol/L S1P triggered the most pronounced proliferation at the 48h (Fig. 5A). Subsequently, SV40 MES 13 cells, induced by S1P under the above mentioned conditions, were co-incubated with COS of varying concentrations and DPs. It was found that COS with a DP of 4 effectively inhibited S1P-induced cell proliferation in a dose-dependent manner without significantly affecting cell survival (Fig. 5B). Therefore, three concentrations of COS with a DP of 4 (1 μmol/L, 5 μmol/L, and 10 μmol/L) were selected for subsequent experiments. Additionally, the optimal concentration of FTY720 is the concentration at which the cell viability is greater than 80% (5 μmol/L) (Fig. 5B). Further investigations using EdU staining demonstrated a significant inhibition of cell proliferation following treatment with FTY720. Moreover, COS exhibited a similar inhibitory effect on cell proliferation (Fig. 5C-D).

3.5 COS promoted cell apoptosis and affected the cell cycle in S1P-induced glomerular mesangial cells

To investigate the relationship between the inhibitory effect of COS on S1P-induced mesangial cells and the cell cycle, the cell cycle assays on different cell treatment groups were performed (Fig. 5E-F). Compared with the control group, the S1P-treated cells showed a significant shortening of the S-phase ($P < 0.001$), from 53.4% to 43.2%, and a significant prolongation of the G2/M-phase ($P < 0.001$), from 10.7% to 20%. While the COS-treated group, as well as the FT720-treated group, showed significant inhibition of the G2/M phase and a considerable accumulation effect on the S phase, there was no significant difference in the G0/G1 phase. The results suggested that COS and FTY720 could affect cell proliferation by modulating the distribution pattern of the cell cycle.

Apoptosis, a physiological process, eliminates harmful cells and regulates cell proliferation, which is crucial for maintaining normal cell turnover. Flow cytometry was employed to investigate whether COS's inhibition of S1P-induced mesangial cells was related to apoptosis. Cells from different treatment groups were double-stained using PI/Annexin V (Fig. 5G-H). After 48h of treatment, S1P induction significantly reduced

cell apoptosis compared to the control group ($P < 0.01$). Conversely, COS and FTY720 significantly increased the apoptotic cell population, impeding cell transition into proliferation.

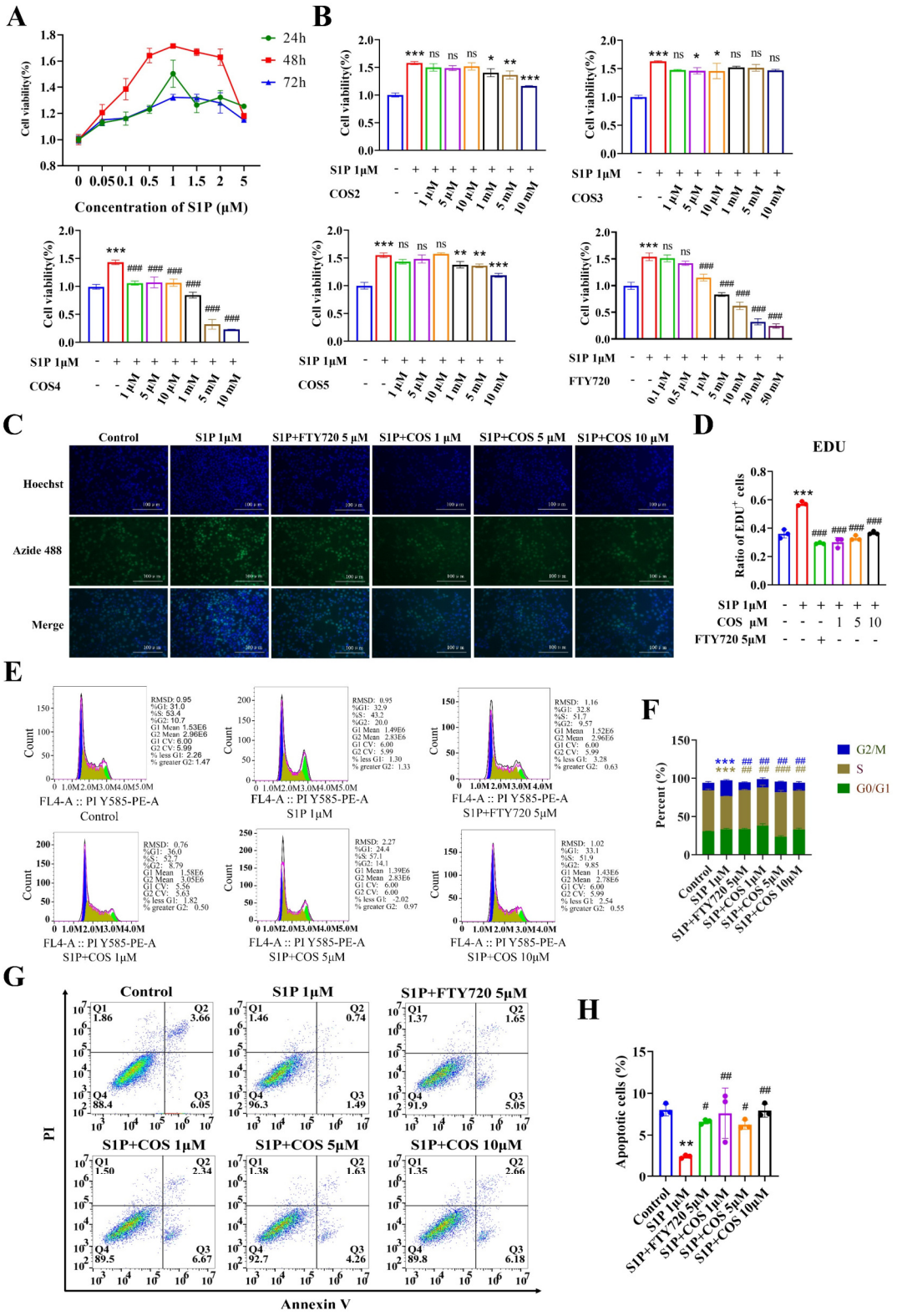

Fig. 5. Anti-proliferative effects of COS on S1P-induced SV40 MES 13 cells (Three independent replicate experiments). (A) Proliferative effect of S1P on SV40 MES 13 cells. (B) Antiproliferative effects of COS with different degrees of polymerization (DPs) (DP 2-5) as well as FTY720 on S1P-induced SV40 MES 13 cell model. (C-D) EdU staining in S1P-induced SV40 MES 13 cells and in the intervention groups. (Scale bar, 100 μm). (E-F) Cell cycle examination by flow cytometry in S1P-induced SV40 MES 13 cells and in the intervention groups. (G-H) Apoptosis examination by flow cytometry in S1P-induced SV40 MES 13 cells as well as in the intervention groups. *$P < 0.05$, **$P < 0.01$, ***$P < 0.001$, and ns represented $P > 0.05$ (compared with control group). # $P < 0.05$, ## $P < 0.01$, ### $P < 0.001$ (compared with S1P-induced group), and ns represented $P > 0.05$.

3.6 COS repressed the expression of inflammation and cell proliferation factors

Furthermore, the effect of S1P on the expression of cellular inflammatory factors, assessing the impact of COS intervention on these responses. Findings revealed that S1P notably increased the gene expression levels and secretion of inflammatory factors ($P < 0.05$) in the cells. COS and FTY720 could significantly inhibit the gene expression of S1P-induced cellular inflammatory factors ($P < 0.05$), while showing a differential effect on their secretion levels (Fig. 6A). COS intervention with 1 μmol/L only had an inhibitory effect on the secretion of IL-1β, while high concentrations of COS intervention significantly attenuated S1P-induced cellular inflammation ($P < 0.05$) (Fig. 6B). Additionally, a notable increase in the gene expression and secretion of proliferative factor PDGF was observed ($P < 0.05$), correlating with S1P's capability to induce cell proliferation (Fig. 6C-D). COS interventions could significantly inhibit the gene expression and the secretion levels of PDGF ($P < 0.05$), while FTY720 shows an effective inhibitory effect on both PDGF and VEGF ($P < 0.05$) (Fig. 6D). Therefore, FTY720 had a more pronounced inhibitory effect on the expression and secretion of inflammatory and proliferative factors.

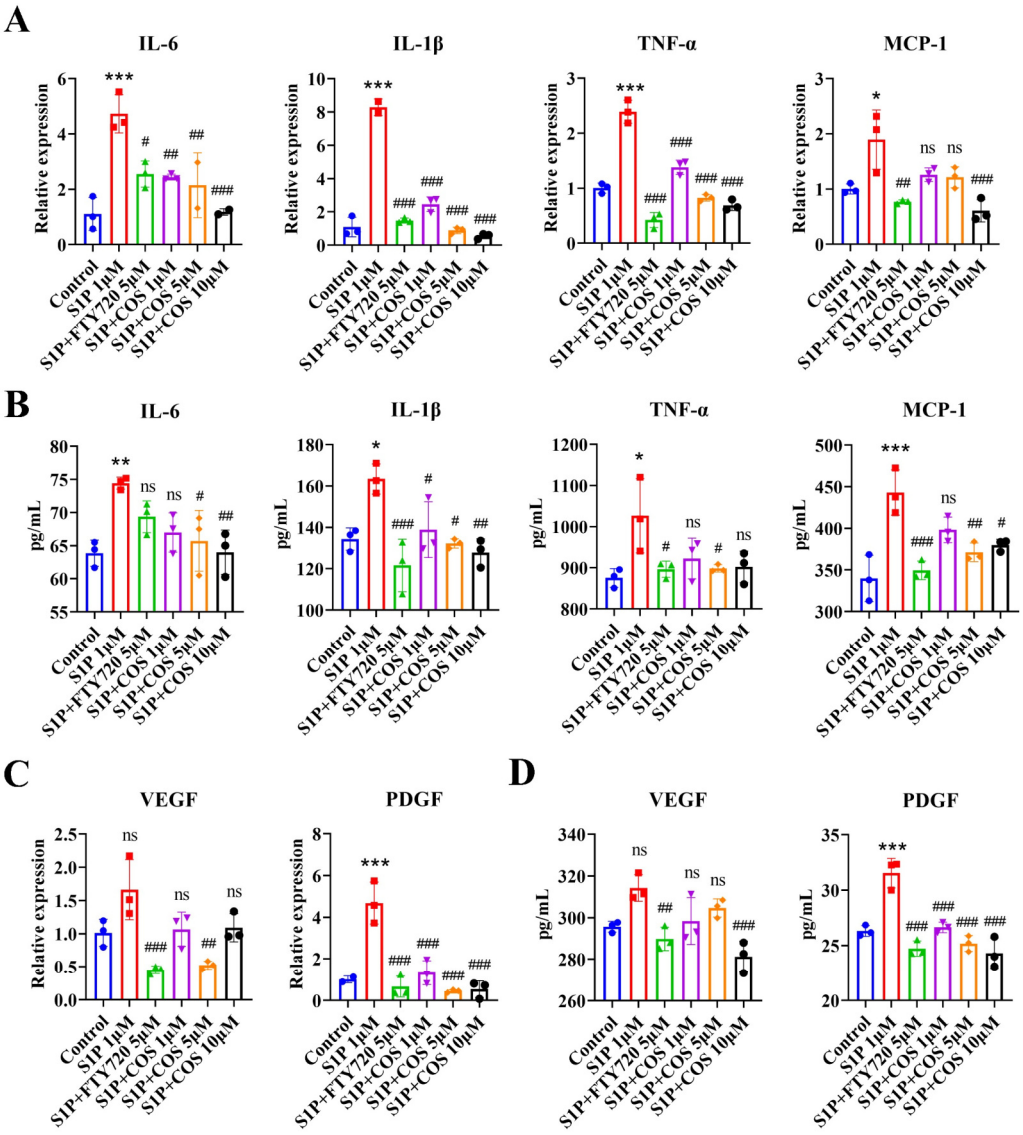

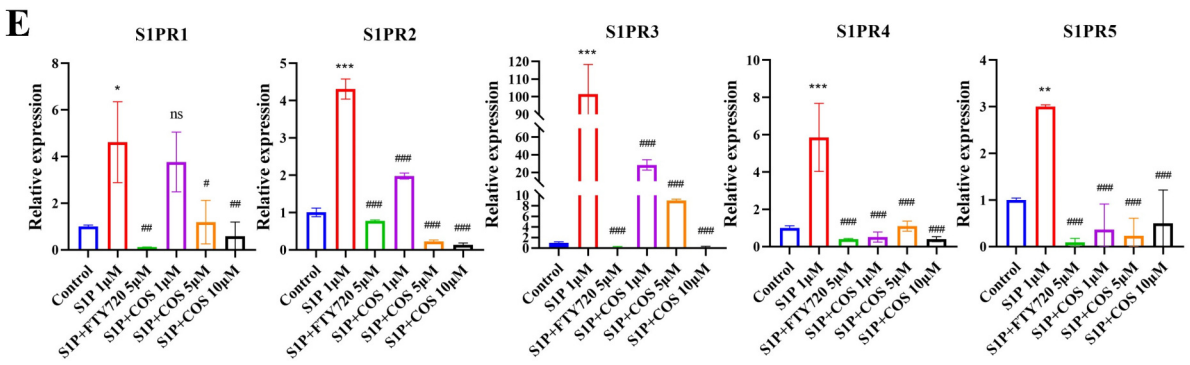

Fig. 6. Anti-inflammatory and anti-proliferative effects of COS on S1P-induced SV40 MES 13 cells (Three independent replicate experiments). (A) Gene expression of cellular inflammatory factors (IL-6, IL-1β, TNF-α, MCP-1) in the S1P induction group and in the intervention group. (B) Quantitative analysis of cellular inflammatory factors. (C) Gene expression of cellular proliferation factors (VEGF, PDGF) in the S1P induction group and in the intervention group. (D) Quantitative analysis of cellular proliferation factors in cell culture supernatants. (E) Effect of COS on S1P-induced gene expression of S1PRs in glomerular mesangial cells. *$P < 0.05$, **$P < 0.01$, ***$P < 0.001$, and ns represented $P > 0.05$ (compared with control group). # $P < 0.05$, ## $P < 0.01$, ### $P < 0.001$ (compared with S1P-induced group), and ns represented $P > 0.05$.

3.7 COS inhibited S1P-induced gene expression of S1PRs in renal mesangial cells

S1P significantly induced the expression of S1PRs in mesenchymal cells, leading to excessive cell proliferation and overexpression of inflammatory factors. FTY720 showed a significant inhibitory effect on the expression of S1PR1-S1PR5 genes ($P < 0.05$) through antagonism of S1P, especially on S1PR1 and S1PR3, with an inhibition rate of more than 98% (Fig. 6E). COS showed a dose-dependent effect on the gene expression of S1PR1-S1PR3 ($P < 0.05$), and the inhibitory effect on their gene expression increased with increasing concentration. The inhibitory effect of COS on the gene expression of S1PR4 and S1PR5 was not dose-dependent. In conclusion, COS reduced the proliferative and inflammatory effects of S1P on mesangial cells by inhibiting the expression of S1PRs, especially S1PR1 and S1PR3. This alleviated the IgAN-like pathological phenotype and cell damage caused by S1P, and may be used as a treatment strategy to control or slow the progression of IgAN.

3.8 COS decelerated renal mesangial proliferation and inflammation in IgAN mice model

Comprehensive assessments were conducted in a murine model to evaluate the potential improvement of chronic renal failure in IgAN through COS intervention with the specific DP (Fig. 7A). PAS staining was employed across all experimental groups to analyze renal structure, while renal function indices and inflammatory factor expression levels were concurrently assessed. Notably, PAS staining revealed significant alterations in the IgAN group, including pronounced glomerular mesangial cell proliferation, extracellular matrix accumulation, glomerular balloon adhesions, and inflammatory cell infiltration (Fig. 7B). Immunofluorescence staining of kidney sections revealed a significant increase in IgA expression in the IgAN mouse model compared to the control group ($P < 0.001$) (Fig. 7C-D). Additionally, the proliferative factors VEGF and PDGF were markedly elevated in the IgAN model ($P < 0.001$) (Fig. 7C, E-F). Intervention with COS or FTY720 significantly reduced the fluorescence intensity of IgA and VEGF, effectively mitigating their deposition in the kidneys.

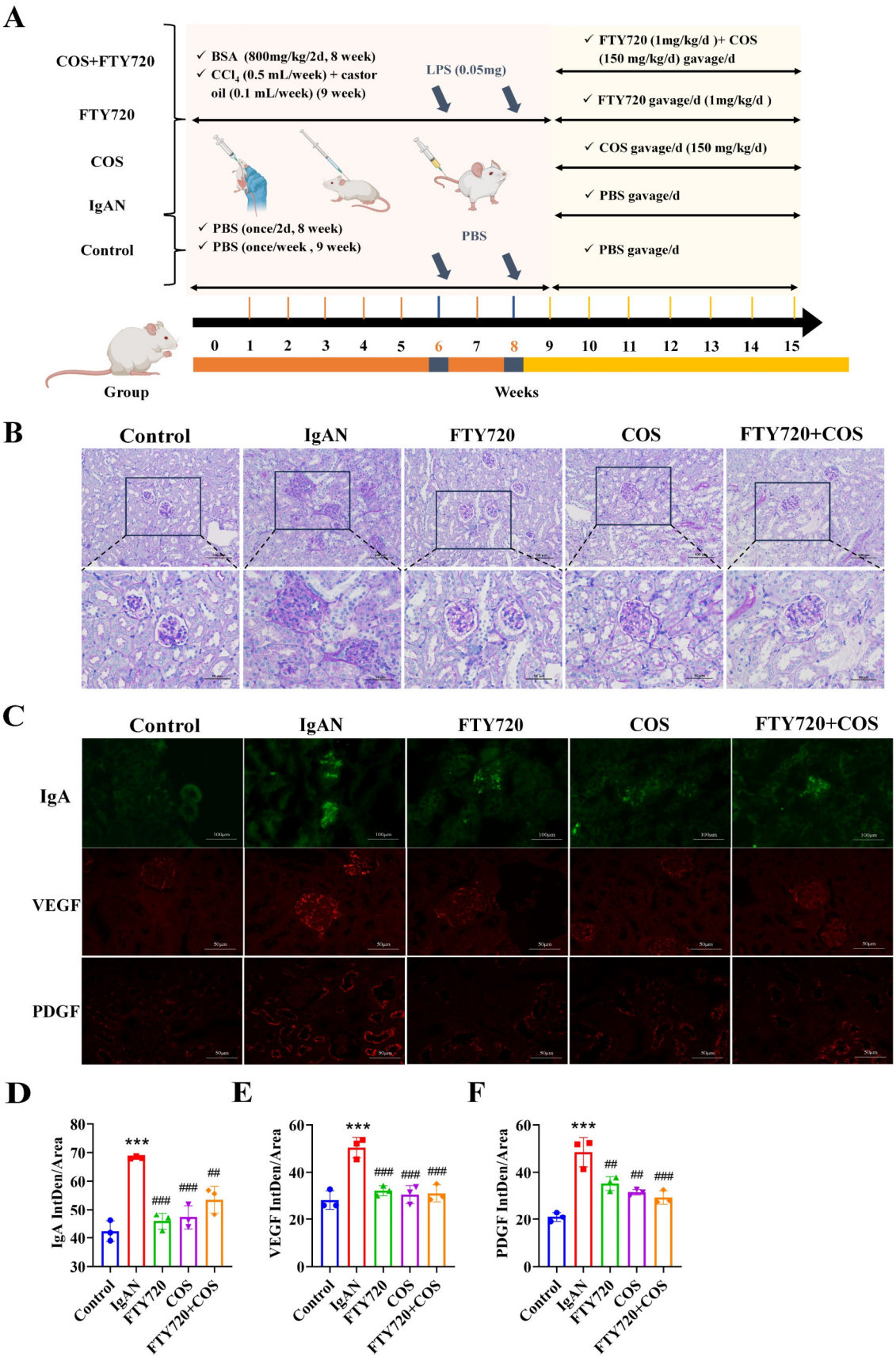

Figure 7. Animal experiment design and the effects of COS on the histopathology of the kidneys in IgAN mice model. (A) Modeling method and grouping of animal experiments. (B) Representative PAS staining of the left kidney of different groups (scale bars, 100 μm and 50 μm) (Three independent replicate experiments). (C-F) Representative immunofluorescent staining (scale bar, 100 μm) of IgA, VEGF, and PDGF in the left kidney and the immunofluorescence quantification of the different groups (Three independent replicate experiments). * $P < 0.05$, ** $P < 0.01$, *** $P < 0.001$ (compared with control group), # $P < 0.05$, ## $P < 0.01$, ### $P < 0.001$ (compared with IgAN model group), and ns represented $P > 0.05$.

Furthermore, examining inflammatory markers in kidney tissues highlighted the efficacy of COS in reducing inflammatory factors. Notably, COS intervention led to significant attenuation in the levels of IL-6 ($P < 0.01$), IL-1β ($P < 0.05$), TNF-α ($P < 0.05$), and MCP-1 ($P < 0.001$), thereby alleviating tissue inflammatory infiltration in the IgAN mouse model (Fig. 8A). The protective effect of COS or FTY720 against renal injury in the IgAN mice model was evaluated by analyzing serum and urine indices from each group (Fig. 8B). Both COS and FTY720 significantly inhibited the elevation of serum uric acid (UA) ($P < 0.001$), BUN ($P < 0.001$), and urine protein/creatinine (UP/UCR) ratio ($P < 0.001$) in the IgAN mice model.

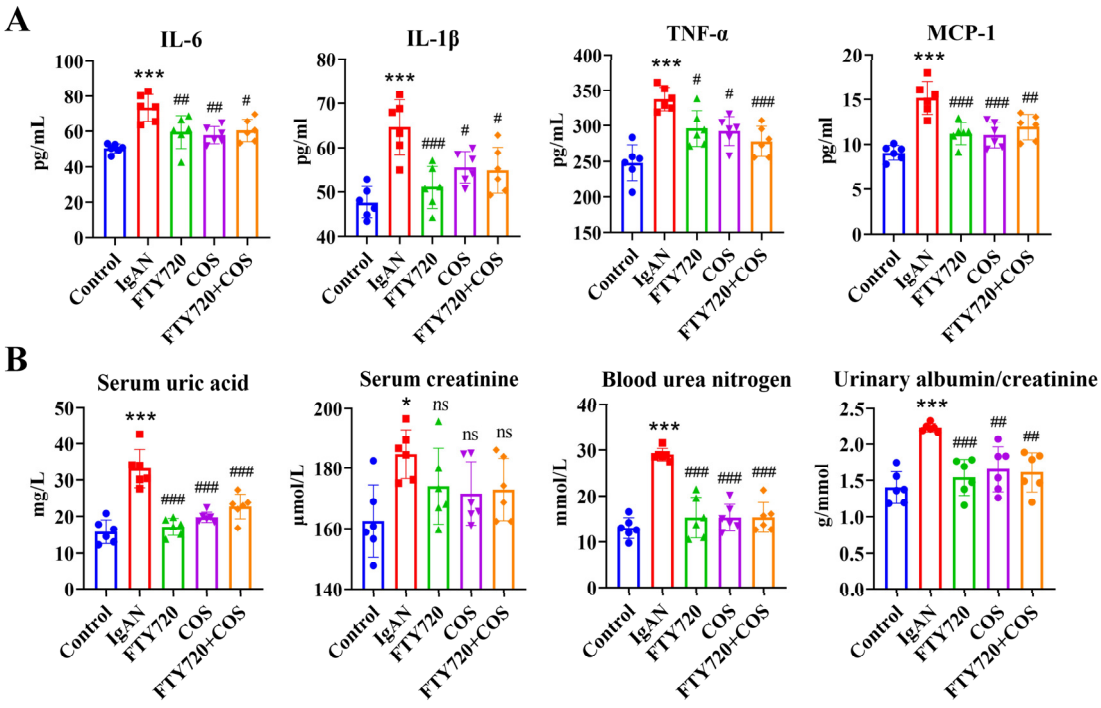

Figure 8. Effects of COS intervention on kidney inflammation and renal function indicators in a mouse model of IgAN. (A) Quantification of inflammatory factors in the kidneys of each group (n=6). (B) Effects of COS and FTY720 interventions on renal functions in IgAN model mice. * $P < 0.05$, ** $P < 0.01$, *** $P < 0.001$ (compared with control group), # $P < 0.05$, ## $P < 0.01$, ### $P < 0.001$ (compared with IgAN model group), and ns represented $P > 0.05$.

3.9 COS modulated S1P levels and S1PRs expression in IgAN mice model

The regulatory effects and mechanisms of COS and FTY720 on S1P levels were further investigated in the IgAN mouse model. The quantitative results showed that the IgAN mice model also exhibited a significant increase in S1P levels compared to the control group ($P < 0.001$). COS exhibited a more effective inhibitory effect on the expression level of S1P ($P < 0.001$) (Fig. 9A). SPHK1 is a crucial rate-limiting and intracellular signaling enzyme for sphingolipid metabolism and plays a central role in producing the lipid signaling molecule S1P [41-43]. The results showed that COS was able to significantly inhibit the secretion of SPHK1 in the kidney (Fig. 9B). Considering the inhibitory effect of COS on S1P production, it can be inferred that COS was able to reduce the production of S1P by inhibiting SPHK1 expression. FTY720 also inhibited SPHK1, with an effect similar to that of COS. S1P exerts its physiological function mainly by binding to the Gi protein-coupled receptors S1PRs (S1PR1-5) [44-46], we then determined the S1PRs expression of different treatment groups in the kidneys (Fig. 9C). COS and FTY720 were both found to significantly inhibit S1PR1

($P < 0.001$) and S1PR3 ($P < 0.001$) expression, with no significant effect on S1PR2, S1PR4, and S1PR5 ($P > 0.05$). The secretion of these two S1P receptor proteins was further examined, and the results consistently demonstrated the inhibitory effect of COS on S1PR1 ($P < 0.01$) and S1PR3 ($P < 0.05$) (Fig. 9D). Further, the intermolecular interaction patterns of COS with S1PR1 and S1PR3 were analyzed using molecular docking, which showed that COS could bind stably to the active pockets of both proteins respectively. COS bound more stably to S1PR1 and was able to form hydrogen bonding interactions with LYS-34, THR-48, GLU-121, PHE-291, and ALA-293 in its active pockets, the docking score was -12.143 (Fig. 9E-F). COS formed hydrogen bonding interactions with TYR-22, GLU-37, THR-42, GLU-115, and ILE-188 of the active pocket of S1PR3, the docking score was -11.599 (Fig. 9G-H). MD simulations showed the stability of COS binding to two proteins (S1PR1 and S1PR3) and the total number of specific contacts with COS that occurred throughout the movement of the proteins, as well as the residue profile of the action (Supplementary Fig. S5). Some residues made more than one specific contact with the ligand, represented by a darker shade of orange, according to the scale to the right of the plot. The MD simulation of FTY720 with S1PR1 and S1PR3 is shown in Supplementary Fig. S6-S7. In conclusion, COS exerted regulatory effects on the S1P signaling pathway by interacting with the S1PR1 and S1PR3 proteins.

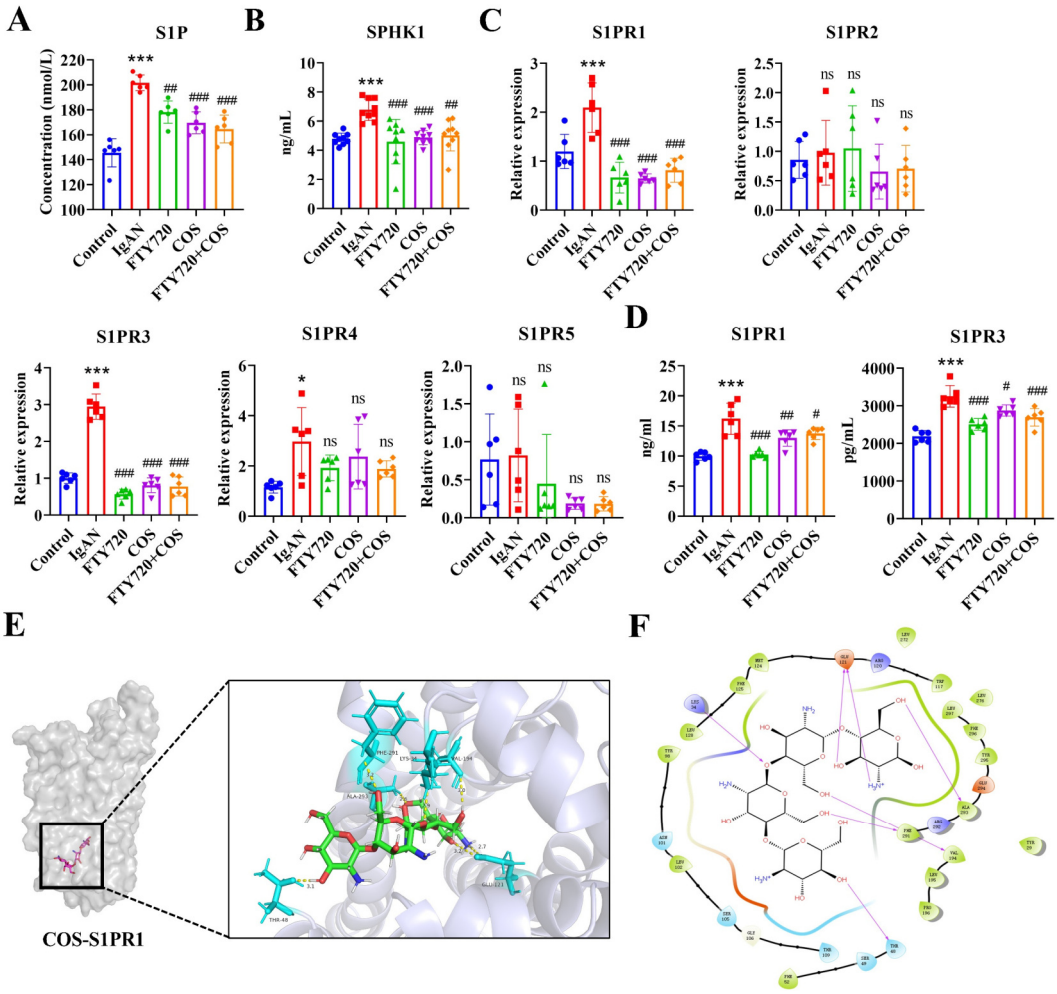

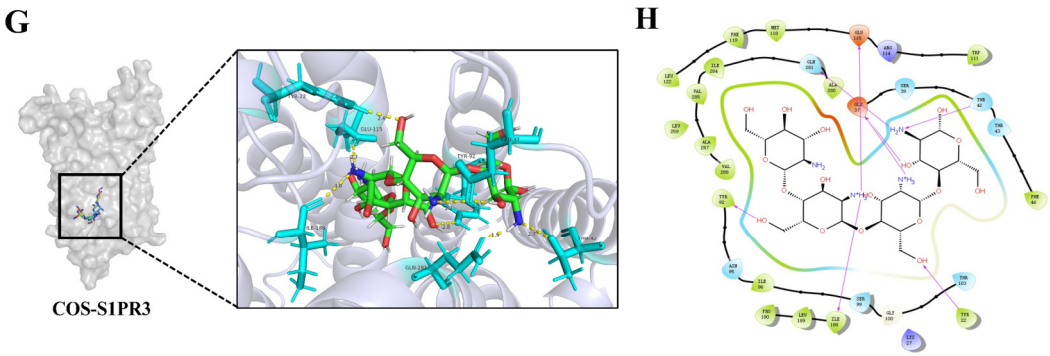

Fig. 9. Regulation of S1PRs by COS. (A) The S1P secretion levels in the IgAN mice model and the intervention groups (n=6). (B) The SPHK1 secretion levels in the kidney in IgAN mice model and the intervention groups (n=6). (C) Gene expression of S1PRs in kidneys in the IgAN mice model and the intervention groups (n=6). (D) The secretion levels of S1PR1 and S1PR3 in kidney tissues (n=6). (E-F) The molecular docking results of COS with S1PR1. (G-H) The molecular docking results of COS with S1PR3. * $P < 0.05$, *** $P < 0.001$ (compared with control group), # $P < 0.05$, ## $P < 0.01$, ### $P < 0.001$ (compared with IgAN model group), and ns represented $P > 0.05$.

4. Discussion

IgAN is the most common primary glomerulonephritis worldwide and the principal cause of ESRD. Traditional IgAN treatment strategies primarily focus on immune modulation and proteinuria control [4, 47]. However, this study highlighted the central role of metabolic abnormalities in IgAN, suggesting that metabolic regulation could serve as a novel intervention strategy. As a naturally derived functional oligosaccharide, COS not only demonstrate excellent safety and biocompatibility but also exhibit unique biological effects, including immunomodulatory, anti-inflammatory, and antioxidant activities. This study revealed that COS effectively ameliorated IgAN pathological phenotypes and renal function by regulating key signaling pathways and metabolic networks. This provided new insights into IgAN treatment and offered scientific support for developing COS as a functional food to treat IgAN.

This study disclosed the metabolic profiles of IgAN patients and discovered a robust correlation between IgAN and metabolic irregularities, clearly differentiating it from the metabolic profile witnessed in healthy individuals. Notably, the most conspicuous variations were observed in serum metabolic abnormalities, effectively discriminating IgAN patients from healthy volunteers and manifesting substantial diagnostic significance. Pathway enrichment analyses revealed remarkable alterations in energy metabolism, including glycerophospholipid metabolism, the TCA cycle, and central carbon metabolism. Notable alterations were also observed in aromatic amino acid metabolism, particularly tryptophan. Additionally, the activation of associated signaling pathways, such as the mTOR signaling pathway and sphingolipid metabolism, was apparent in IgAN patients. In this study, we used QC samples, randomization of sample injection order and permutation test to reduce false positive results caused by technical errors or data bias. We also verified the correlation between the selected metabolic markers and clinical indicators through ROC curve analysis and correlation analysis (Spearman's rank correlation analysis) to improve the reliability of the results. Results have shown that the important bioactive lipid S1P was associated with the pathogenesis and progression of IgAN. The significantly elevated S1P in IgAN patients was closely related to renal function indicators (including 24h-Upro, Cys-C, BUN, Scr and eGFR) and cytokines (IgA1, IL-4, IL-6, TNF-α and IL-17).

Sphingolipids (including ceramides and S1P) are important lipid signaling molecules in disease and health [43]. Originating from sphingosine metabolism, S1P intricately regulates cellular proliferation, intercellular signaling, and inflammatory responses [48]. We have observed a metabolic disorder of S1P in IgAN patients. Specifically, S1P levels were significantly elevated, while SPH levels were markedly reduced, and ceramide levels remained unchanged. This suggested an interruption in the conversion of ceramide to sphingosine. Sphingosine was a critical intermediate in the sphingolipid metabolic pathway, and its conversion to S1P played a crucial role in immune regulation and inflammation—both of which were central to the pathogenesis of IgAN [49]. The observed decrease in SPH levels indicated a reduced availability of this metabolite for conversion into S1P, potentially leading to impaired S1P signaling. Hexadecanoic acid and PE were vital constituents of the cellular membrane. The reduction of the fatty acids and the disruption in PE levels could result in impaired cellular signaling, thereby exacerbating the inflammatory processes associated with IgAN [50,51]. This study revealed that S1P can serve as a metabolic target in IgAN, promoting excessive proliferation and inflammation of glomerular mesangial cells by activating S1PRs. S1P primarily exerted its physiological effects by binding to G-protein-coupled S1PRs (S1PR1–5). In an *in vitro* cell model, S1P significantly stimulated the overexpression of S1PRs in glomerular mesangial cells, particularly S1PR1 and S1PR3. Activation of S1PRs triggered excessive mesangial cell proliferation and overexpression of proliferation factors (VEGF, PDGF) as well as inflammatory cytokines (IL-6, TNF-α, IL-1β, and MCP-1) ($P < 0.05$). These S1P-induced biological effects in glomerular mesangial cells closely resemble the pathological phenotypes of IgAN, underscoring the critical role of S1P in the pathogenesis of IgAN.

FTY720, an approved modulator of S1PRs receptors, particularly S1PR1[52], exhibited promising therapeutic effects in various autoimmune diseases and in regulating inflammation [53,54,55]. This study included an FTY720 intervention group as a positive control. COS possess diverse bioactivities, including anti-inflammatory, anti-tumor, immune-regulatory, and lipid-regulatory properties. Moreover, COS with different DPs have significantly different structure-activity relationships. This study investigated the effects and mechanisms of COS with different DPs on S1P-induced IgAN-like phenotypes in glomerular mesangial cells. The results demonstrated that COS with specific DP effectively blocked cell cycle progression from the S phase to the G2/M phase and increased the apoptotic cell population. This ultimately suppressed excessive cell proliferation, producing effects similar to those of FTY720. In addition, COS significantly reduced the expression levels of proliferation and inflammatory factors ($P < 0.05$), effectively mitigating S1P-induced cellular pathology. Further investigations revealed that COS significantly downregulated the gene expression of S1PRs in S1P-induced mesangial cells ($P < 0.05$), with the strongest dose-dependent inhibitory effects observed on S1PR1 and S1PR3. *In vivo* experiments showed that COS significantly inhibited the expression of SPHK1 and suppressed the production of S1P in the kidneys of IgAN mice. This alleviated the excessive accumulation of S1P at the metabolic level during the pathology of IgAN. SPHK inhibitors were reported to show promising anti-tumor efficacy against hematological cancers by reducing S1P levels [56]. In addition, COS inhibited the abnormal activation of downstream signal pathways by

inhibiting the gene and protein expression of S1PR1 and S1PR3, and by blocking the binding of S1P to the receptor through molecular docking competition. Molecular interaction analysis showed that COS bound to the active sites of S1PR1 and S1PR3, with significant differences in binding affinity and interacting residues. COS bound more strongly to S1PR1 (docking score -12.143), and the binding site included LYS-34, THR-48, GLU-121, PHE-291 and ALA-293, of which PHE-291 and ALA-293 further enhanced the stability of the binding through hydrogen bonding and hydrophobic interactions. COS bound to S1PR3 with a slightly lower affinity (docking score -11.599), mainly through the TYR-22 and GLU-37 sites. Furthermore, the docking simulation results showed that COS and S1PR1 had a higher number of hydrogen bond contacts and lower values of RMSD. The differences in binding affinity and sites directly explained the different strengths of COS effects on proliferation and inflammation regulation in *in vitro* and *in vivo* experiments. This finding provided a basis for further research into the specific mechanism of action of COS and the S1P signaling pathway.

5. Conclusion

This study highlighted S1P as a potential key diagnostic marker for IgAN. COS exhibited effects similar to those of S1P antagonist FY720 by inhibiting the S1PR1/S1PR3 pathway, thereby reducing mesangial cell proliferation and inflammation in IgAN. However, this study has some limitations in terms of sample size and downstream mechanisms of S1P signaling pathway. Future studies will integrate multi-centre data and increase the sample size to further verify the value of S1P in the diagnosis of IgAN. In addition, we will further investigate the mechanism of COS on key enzymes and molecules in the S1P pathway. Nevertheless, these findings provide a feasible approach for IgAN treatment and management, suggesting that targeting S1P metabolism could offer new therapeutic options. Furthermore, the study supported the potential of COS as a functional food for improving IgAN outcomes.

Finding

This work was supported by the Shanghai Post-doctoral Excellence Program (2022153), Natural Science Foundation of Shanghai (23ZR1415400), 111 Project (B18022), Shanghai Frontiers Science Center of Optogenetic Techniques for Cell Metabolism (Shanghai Municipal Education Commission), Shanghai Collaborative Innovation Center for Biomanufacturing Technology. The work was also supported by National Natural Science Foundation of China (No. 82304948), Natural Science Foundation in Minhang District of Shanghai (2022MHZ004), Minhang District High-Level Specialty Key Physician Training Program (2020MZYS19) and Hospital-level Discipline-Chronic Disease Group-Chronic Kidney Disease Project (YJXK-2021-13).

Data and materials availability

All data are available in the main text or the supplemental information.

Conflict of interest

The authors declare that they have no known competing financial interests or personal relationships that could have appeared to influence the work reported in this paper.

References

[1] Zhang H, Barratt J, Is IgA nephropathy the same disease in different parts of the world? Semin. Immunopathol. 43 (5) (2021) 707-715. https://doi.org/10.1007/s00281-021-00884-7.

[2] Pattrapornpisut P, Avila-Casado C, Reich H N, IgA nephropathy: core curriculum 2021, Am. J. Kidney Dis. 78 (3) (2021) 429-441. https://doi.org/10.1053/j.ajkd.2021.01.024.

[3] Fellström BC, Barratt J, Cook H, et al., Targeted-release budesonide versus placebo in patients with IgA nephropathy (NEFIGAN): a double-blind, randomised, placebo-controlled phase 2b trial, Lancet 389 (10084) (2017) 2117. https://doi.org/10.1016/S0140-6736(17)30550-0.

[4] Rajasekaran A, Julian BA, Rizk DV, IgA nephropathy: an interesting autoimmune kidney disease, Am. J. Med. Sci. 361 (2) (2021) 176-194. https://doi.org/10.1016/j.amjms.2020.10.003.

[5] Berthoux F, Suzuki H, Thibaudin L, et al., Autoantibodies targeting galactose-deficient IgA1 associate with progression of IgA nephropathy, J. Am. Soc. Nephrol. 23 (9) (2012) 1579. https://doi.org/10.1681/ASN.2012010053.

[6] Chen P, Yu G, Zhang X, et al., Plasma galactose-deficient IgA1 and C3 and CKD progression in IgA nephropathy, Clin. J. Am. Soc. Nephrol. 14 (10) (2019) 1458. https://doi.org/10.2215/CJN.13711118.

[7] Pereira PR, Carrageta DF, Oliveira PF, et al., Metabolomics as a tool for the early diagnosis and prognosis of diabetic kidney disease, Med. Res. Rev. 42 (4) (2022) 1518-1544. https://doi.org/10.1002/med.21883.

[8] Dahabiyeh LA, Nimer RM, Sumaily KM, et al., Metabolomics profiling distinctively identified end-stage renal disease patients from chronic kidney disease patients, Sci. Rep. 13 (1) (2023) 6161. https://doi.org/10.1038/s41598-023-33377-8.

[9] Hu JR, Myint L, Levey AS, et al., A metabolomics approach identified toxins associated with uremic symptoms in advanced chronic kidney disease, Kidney Int. 101 (2) (2022) 369-378. https://doi.org/10.1016/j.kint.2021.10.035.

[10] Wu H, Tang D, Yun M, et al., Metabolic dysfunctions of intestinal fatty acids and tryptophan reveal immuno-inflammatory response activation in IgA nephropathy, Front. Med. 9 (2022) 811526. https://doi.org/10.3389/fmed.2022.811526.

[11] Li J, Cao Y, Lu R, et al., Integrated fecal microbiome and serum metabolomics analysis reveals abnormal changes in rats with immunoglobulin A nephropathy and the intervention effect of Zhen Wu Tang, Front. Pharmacol. 11 (2021) 606689. https://doi.org/10.3389/fphar.2020.606689.

[12] Moresco RN, Speeckaert MM, Delanghe JR, Diagnosis and monitoring of IgA nephropathy: the role of biomarkers as an alternative to renal biopsy, Autoimmun. Rev. 14 (10) (2015) 847-853. https://doi.org/10.1016/j.autrev.2015.05.009.

[13] Dong L, Tan J, Zhong Z, et al., Altered serum metabolic profile in patients with IgA nephropathy, Clin. Chim. Acta 549 (2023) 117561. https://doi.org/10.1016/j.cca.2023.117561.

[14] Park S, Lee J, Yang SH, et al., Comprehensive metabolomic profiling in early IgA nephropathy patients reveals urine glycine as a prognostic biomarker, J. Cell. Mol. Med. 25 (11) (2021) 5177. https://doi.org/10.1111/jcmm.16520.

[15] Deng Y, Wu Q, Chen W, et al., Lipidomics reveals association of circulating lipids with body mass index and outcomes in IgA nephropathy patients, J. Mol. Cell Biol. 13 (8) (2021) 565-575. https://doi.org/10.1093/jmcb/mjab040.

[16] Chen YY, Chen DQ, Chen L, et al., Microbiome–metabolome reveals the contribution of gut–kidney axis on kidney disease, J. Transl. Med. 17 (2019) 1-11. https://doi.org/10.1186/s12967-018-1756-4.

[17] Wang F, Li N, Ni S, et al., The Effects of Specific Gut Microbiota and Metabolites on IgA Nephropathy—Based on Mendelian Randomization and Clinical Validation, Nutrients 15 (10) (2023) 2407. https://doi.org/10.3390/nu15102407.

[18] Li J, Cao Y, Lu R, et al., Integrated fecal microbiome and serum metabolomics analysis reveals abnormal changes in rats with immunoglobulin A nephropathy and the intervention effect of Zhen Wu Tang, Front. Pharmacol. 11 (2021) 606689. https://doi.org/10.3389/fphar.2020.606689.

[19] Liaqat F, Eltem R, Chitooligosaccharides and their biological activities: A comprehensive review, Carbohydr. Polym. 184 (2018) 243-259. https://doi.org/10.1016/j.carbpol.2017.12.067.

[20] Zhai X, Li C, Ren D, et al., The impact of chitooligosaccharides and their derivatives on the in vitro and in vivo antitumor activity: A comprehensive review, Carbohydr. Polym. 266 (2021) 118132. https://doi.org/10.1016/j.carbpol.2021.118132.

[21] Chen Y, Ling Z, Wang X, et al., The beneficial mechanism of chitosan and chitooligosaccharides in the intestine on different health status, J. Funct. 97 (2022) 105232. https://doi.org/10.1016/j.jff.2022.105232.

[22] Liu Y, Zhang R, Zou J, et al., The impact of chitooligosaccharides with a certain degree of polymerization on diabetic nephropathic mice and high glucose-damaged HK-2 cells, Food Sci. Nutr. 12 (6) (2024) 4173–4184. https://doi.org/10.1002/fsn3.4078.

[23] Wang Y, Ji X, Zhao M, et al., Modulation of tryptophan metabolism via AHR-IL22 pathway mediates the alleviation of DSS-induced colitis by chitooligosaccharides with different degrees of polymerization, Carbohydr. Polym. 319 (2023) 121180. https://doi.org/10.1016/j.carbpol.2023.121180.

[24] Beckwith H, Medjeral-Thomas N, Galliford J, et al., Mycophenolate mofetil therapy in immunoglobulin A nephropathy: histological changes after treatment, Nephrol. Dial. Transplant. 32 (suppl_1) (2017) 123-128. https://doi.org/10.1093/ndt/gfw326.

[25] Joher N, Gosset C, Guerrot D, et al., Immunoglobulin A nephropathy in association with inflammatory bowel diseases: results from a national study and systematic literature review, Nephrol. Dial. Transpl. 37 (3) (2022) 531-539. https://doi.org/10.1093/ndt/gfaa378.

[26] Han L, Zhao L, Zhou Y, et al., Altered metabolome and microbiome features provide clues in understanding irritable bowel syndrome and depression comorbidity, ISME J. 16 (4) (2022) 983-996. https://doi.org/10.1038/s41396-021-01123-5.

[27] Ji X, Zhu L, Chang K, et al., Chitooligosaccahrides: Digestion characterization and effect of the degree of polymerization on gut microorganisms to manage the metabolome functional diversity *in vitro*, Carbohydr. Polym. 275 (2022) 118716. https://doi.org/10.1016/j.carbpol.2021.118716.

[28] Liu H, Xu F, Gao Y, et al., An integrated LC-MS/MS strategy for quantifying the oxidative-redox metabolome in multiple biological samples, Anal. Chem. 92 (13) (2020) 8810-8818. https://doi.org/10.1021/acs.analchem.0c00242.

[29] Tan J, Dong L, Jiang Z, et al., Probiotics ameliorate IgA nephropathy by improving gut dysbiosis and blunting NLRP3 signaling, Transl. Med. 20 (1) (2022) 1-16. https://doi.org/10.1186/s12967-022-03585-3.

[30] Zhao L, Lan Z, Peng L, et al., Triptolide promotes autophagy to inhibit mesangial cell proliferation in IgA nephropathy via the CARD9/p38 MAPK pathway, Cell Prolif. 55 (9) (2022) e13278. https://doi.org/10.1111/cpr.13278.

[31] Shi Y, Shi X, Zhao M, et al., Pharmacological potential of Astragali Radix for the treatment of kidney diseases, Phytomedicine 123 (2023) 155196. https://doi.org/10.1016/j.phymed.2023.155196.

[32] Wang LY, Sun XJ, Wang C, et al., Sphingosine-1-phosphate receptor modulator FTY720 attenuates experimental myeloperoxidase-ANCA vasculitis in a T cell-dependent manner, Clin. Sci. 134 (12) (2020) 1475-1489. https://doi.org/10.1042/CS20200497.

[33] Lankadasari MB, Aparna JS, Mohammed S, et al., Targeting S1PR1/STAT3 loop abrogates desmoplasia and chemosensitizes pancreatic cancer to gemcitabine, Theranostics 8 (14) (2018) 3824. https://doi.org/10.7150/thno.25308.

[34] Kappos L, Antel J, Comi G, et al., Oral fingolimod (FTY720) for relapsing multiple sclerosis, N. Engl. J. Med. 355 (11) (2006) 1124-1140. http://doi.org/10.1056/NEJMoa052643.

[35] Hao W, Li K, Ge X, et al., The effect of N-acetylation on the anti-inflammatory activity of chitooligosaccharides and its potential for relieving endotoxemia, Int. J. Mol. Sci. 23 (15) (2022) 8205. https://doi.org/10.3390/ijms23158205.

[36] Bowers KJ, Chow E, Xu H, et al., Scalable algorithms for molecular dynamics simulations on commodity clusters, in Proc. 2006 ACM/IEEE Conference on Supercomputing, New York (2006) 84-es. https://doi.org/10.1145/1188455.1188544.

[37] Seikrit C, Pabst O, The immune landscape of IgA induction in the gut, Semin. Immunopathol. 43 (5) (2021) 627-637. https://doi.org/10.1007/s00281-021-00879-4.

[38] He JW, Zhou XJ, Lv JC, et al., Perspectives on how mucosal immune responses, infections and gut microbiome shape IgA nephropathy and future therapies, Theranostics 10 (25) (2020) 11462. https://doi.org/10.7150/thno.49778.

[39] Liang H, Wang M, Wen Y, et al., Predicting acute pancreatitis severity with enhanced computed tomography scans using convolutional neural networks, Sci. Rep. 13 (1) (2023) 17514. https://doi.org/10.1038/s41598-023-44828-7.

[40] Endre ZH, Pickering JW, Walker RJ, et al., Improved performance of urinary biomarkers of acute kidney injury in the critically ill by stratification for injury duration and baseline renal function, Kidney Int. 79 (10) (2011) 1119. https://doi.org/10.1038/ki.2010.555.

[41] Wang D, Han S, Lv G, et al., Pancreatic acinar cells-derived sphingosine-1-phosphate contributes to fibrosis of chronic pancreatitis via inducing autophagy and activation of pancreatic stellate cells, Gastroenterology 165 (6) (2023) 1488-1504. https://doi.org/10.1053/j.gastro.2023.08.029.

[42] Jozefczuk E, Guzik TJ, Siedlinski M, Significance of sphingosine-1-phosphate in cardiovascular physiology and pathology, Pharmacol. Res. 156 (2020) 104793. https://doi.org/10.1016/j.phrs.2020.104793.

[43] Green CD, Maceyka M, Sphingolipids in metabolic disease: The good, the bad, and the unknown, Cell Metab. 33 (7) (2021) 1293-1306. https://doi.org/10.1016/j.cmet.2021.06.006.

[44] Yuan Y, Jia G, Wu C, et al., Structures of signaling complexes of lipid receptors S1PR1 and S1PR5 reveal mechanisms of activation and drug recognition, Cell Res. 31 (12) (2021) 1263-1274. https://doi.org/10.1038/s41422-021-00566-x.

[45] Mohammed S, Bindu A, Viswanathan A, et al., Sphingosine 1-phosphate signaling during infection and immunity, Prog. Lipid Res. 92 (2023) 101251. https://doi.org/10.1016/j.plipres.2023.101251.

[46] Burg N, Salmon JE, Hla T, Sphingosine 1-phosphate receptor-targeted therapeutics in rheumatic diseases, Nat. Rev. Rheumatol. 18 (6) (2022) 335-351. https://doi.org/10.1038/s41584-022-00784-6.

[47] Maixnerova D, Tesar V, Emerging modes of treatment of IgA nephropathy, Int. J. Mol. Sci. 21 (23) (2020) 9064. https://doi.org/10.3390/ijms21239064.

[48] Cartier A, Hla T, Sphingosine 1-phosphate: Lipid signaling in pathology and therapy, Science 366 (6463) (2019) eaar5551. https://doi.org/10.1126/science.aar5551.

[49] Quinville BM, Deschenes NM, Ryckman AE, et al., A comprehensive review: sphingolipid metabolism and implications of disruption in sphingolipid homeostasis, Int. J. Mol. Sci. 22 (11) (2021) 5793. https://doi.org/10.3390/ijms22115793.

[50] Astudillo AM, Balboa MA, Balsinde J, Compartmentalized regulation of lipid signaling in oxidative stress and inflammation: Plasmalogens, oxidized lipids and ferroptosis as new paradigms of bioactive lipid research, Prog. Lipid Res. 89 (2023) 101207. https://doi.org/10.1016/j.plipres.2022.101207.

[51] Patel D, Witt SN, Ethanolamine and phosphatidylethanolamine: partners in health and disease, Oxid. Med. Cell. Longev. 2017 (2017) 4829180. https://doi.org/10.1155/2017/4829180.

[52] Stepanovska B, Huwiler A, Targeting the S1P receptor signaling pathways as a promising approach for treatment of autoimmune and inflammatory diseases, Pharmacol. Res. 154 (2020) 104170. https://doi.org/10.1016/j.phrs.2019.02.009.

[53] Hannun YA, Obeid LM, Sphingolipids and their metabolism in physiology and disease, Nat. Rev. Mol. Cell Biol. 19 (3) (2018) 175-191. https://doi.org/10.1016/j.cmet.2021.06.006.

[54] Stockstill K, Doyle TM, Yan X, et al., Dysregulation of sphingolipid metabolism contributes to bortezomib-induced neuropathic pain, J. Exp. Med. 215 (5) (2018) 1301-1313. https://doi.org/10.1084/jem.20170584.

[55] El Alwani M, Wu BX, Obeid LM, et al., Bioactive sphingolipids in the modulation of the inflammatory response, Pharmacol. Therapeut. 112 (1) (2006) 171-183. https://doi.org/10.1016/j.pharmthera.2006.04.004.

[56] Evangelisti C, Buontempo F, Lonetti A, et al., Therapeutic potential of targeting sphingosine kinases and sphingosine 1-phosphate in hematological malignancies, Leukemia. 30 (11) (2016) 2142-2151. https://doi.org/10.1038/leu.2016.208.